Increased atherosclerosis and expression of inflammarafts in macrophage foam cells in AIBP-deficient mice

Shenglin Li[1], Nicolaus Nazarenkov[1], Elena Alekseeva[1], Juliana M. Navia-Pelaez[1], Patrick Secrest[1], Philip L.S.M. Gordts[1,2,3,4], Sven Heinz[1], Yury I. Miller[1*]

[1] Department of Medicine, University of California, San Diego, La Jolla, CA, USA.

[2] Glycobiology Research and Training Center, University of California, San Diego, La Jolla, CA, USA.

[3] University of Utah Molecular Medicine Program, University of Utah, Salt Lake City, UT, USA,

[4] Department of Pathology, Division of Microbiology & Immunology, University of Utah School of Medicine, Salt Lake City, UT, USA

* Correspondence should be addressed to: University of California, San Diego, 9500 Gilman Drive, La Jolla, CA 92093-0682. Email: yumiller@health.ucsd.edu

Running title: **Inflammatory foam cell in AIBP-deficient mice**

Abstract

Background: Atherosclerotic lesions comprise different populations of macrophages, including lipid-laden macrophage foam cells and non-foamy, inflammatory macrophages, playing different roles in disease progression. Previous studies demonstrated higher expression of inflammarafts – enlarged, cholesterol-rich lipid rafts hosting assemblies of inflammatory receptors – in non-foamy, inflammatory macrophages, as opposed to lower inflammarafts in lipid-lade macrophage foam cells. Apolipoprotein A-I Binding Protein (AIBP) facilitates cholesterol efflux from macrophages and has been shown to reduce inflammatory responses and protect against atherosclerosis. This study investigated the effect of AIBP deficiency on inflammaraft expression in aortic foam cells and non-foamy macrophages in hypercholesterolemic mice.

Methods: Single-cell suspensions were prepared from aortae of *Apoa1bp*$^{-/-}$*Ldlr*$^{-/-}$ and *Ldlr*$^{-/-}$ male and female mice fed a high-cholesterol, high-fat diet. CD45^{+} F4/80^{+} macrophages were gated for BODIPY-high foamy and BODIPY-low non-foamy cells and analyzed for the expression of inflammaraft markers TLR4 (toll-like receptor-4) dimers and lipid rafts. Consecutive sections of the aortic root were stained with modified Van Gieson stain to assess lesion and necrotic core sizes.

Results: Foam cells constituted a higher percentage of macrophages and contained more neutral lipid in *Apoa1bp*$^{-/-}$*Ldlr*$^{-/-}$ compared to *Ldlr*$^{-/-}$ aorta. Importantly, in AIBP-deficient mice, foam cells expressed higher levels of TLR4 dimers and lipid rafts than in control mice, while non-foamy cells expressed similar levels. *Apoa1bp*$^{-/-}$*Ldlr*$^{-/-}$ mice had larger atherosclerotic lesions and necrotic cores compared to *Ldlr*$^{-/-}$ mice. Male and female mice showed similar results.

Conclusions: Our results indicate that AIBP deficiency leads to the formation of a new foam cell phenotype in which the increased lipid accumulation is associated with an increased expression of TLR4 inflammarafts. This transition of foam cells to a proinflammatory phenotype correlates with the development of advanced atherosclerotic plaques.

Keywords: atherosclerosis, lipid rafts, inflammarafts, AIBP, TLR4, macrophage foam cell

Non-standard Abbreviations and Acronyms

ABC	ATP-binding cassette transporter
AIBP	apolipoprotein A-I binding protein
HDL	high-density lipoprotein
IL	interleukin
LPS	lipopolysaccharide
MCP-1	monocyte chemoattractant protein-1
oxLDL	oxidized low-density lipoprotein
TLR4	toll-like receptor-4

Introduction

The advances in flow cytometry and sequencing techniques have helped identify distinct populations of macrophages in human and mouse atherosclerotic lesions.[1,2] One differentiating feature in lesional macrophages is the handling of excess cholesterol. Lipid-laden macrophage foam cells accumulate large deposits of esterified cholesterol in lipid droplets. In contrast, non-foamy macrophages display increased levels of unesterified cholesterol-rich lipid rafts in the plasma membrane, which due to the low diffusion rates and the presence of cholesterol and sphingolipid binding domains in many proteins, serve as a platform for the assembly of functional receptor complexes.[3] Enlarged lipid rafts that host assembled complexes of inflammatory receptors are called inflammarafts.[4] In atherosclerotic lesions, non-foamy macrophages, which express inflammatory genes [1], retain high levels of inflammarafts, particularly inflammarafts rich in TLR4 (toll-like receptor-4) dimers.[3] In contrast, macrophage foam cells express lipid storage genes, have low expression of inflammatory genes [1] and low abundance of TLR4 inflammarafts.[3]

To study the regulation of the TLR4 inflammaraft expression between foamy and non-foamy macrophages in atherosclerotic lesions, we compared their phenotypes in *Ldlr*$^{-/-}$ and *Apoa1bp*$^{-/-}$*Ldlr*$^{-/-}$ mice. Apolipoprotein A-I binding protein (AIBP, gene name *Apoa1bp* or *Naxe*) facilitates cholesterol efflux by binding to apoA-I to stabilize ATP-binding cassette transporter A1 (ABCA1) and to TLR4 to target the cholesterol efflux machinery to TLR4-expressing inflammatory cells.[5-7] AIBP is ubiquitously expressed and can be secreted in response to apoA-I or oxidized LDL.[8,10] Intracellular AIBP localizes to mitochondria and regulates mitophagy.[9,10] *Apoa1bp*$^{-/-}$*Ldlr*$^{-/-}$ mice fed a high-cholesterol, high-fat diet have more atherosclerosis compared to *Ldlr*$^{-/-}$ mice.[11] In mouse models of neuropathic pain and Alzheimer's disease, *Apoa1bp*$^{-/-}$ mice have

chronic, increased expression of TLR4 inflammarafts in spinal cord or brain microglia, respectively, accompanied by oxidative stress and mitochondrial dysfunction.[12,13]

Here, we demonstrate that systemic AIBP deficiency in hyperlipidemic mice results in a surprising proinflammatory phenotypic switch in macrophage foam cells, characterized by increased lipid accumulation and increased expression of TLR4 inflammarafts, as well as larger necrotic core sizes of atherosclerotic lesions.

Methods

Animals

Apoa1bp$^{-/-}$*Ldlr*$^{-/-}$ mice [11] and *Ldlr*$^{-/-}$ mice were bred in-house and housed at a maximum of five animals of the same sex per cage at room temperature and a 12:12 light-dark cycle. Age- and weight-matched mice were used. Both male and female mice were included. Starting at eight weeks of age, mice were fed a 16-week Western-style diet containing 42% kcal from fat and 0.2% cholesterol (TD.88137, Envigo Teklad). Mice were fasted for 8 hours before euthanasia. Blood was drawn through cardiac puncture and collected in EDTA-containing vials. Mice were then perfused with 10 mL ice-cold PBS containing 2 mM EDTA; aortae were dissected and prepared for flow cytometry analyses. All experiments were conducted according to a protocol approved by the Institutional Animal Care and Use Committee at the University of California, San Diego.

Quantification of atherosclerotic lesions

Hearts were fixed and embedded in paraffin for the assessment of atherosclerosis as described previously. [3] Briefly, consecutive 10 μm-thick aortic cross-sections were collected in 100 μm increments starting from the first appearance of the first leaflet of the aortic valve until the last leaflet. Sections were stained with modified Van Gieson staining to enhance the contrast between

the intima and surrounding tissues. Images were acquired using a Nano Zoomer Slide Scanner. At each 100 μm increment, the lesion size and necrotic core size in each mouse were analyzed by computer-assisted morphometry (Image-Pro Plus 6.3, Media Cybernetics) by two investigators blinded to the study protocol. Lesion and necrotic core volumes were analyzed by calculating the area under the curve in each mouse.

Measurements of cholesterol and triglycerides

Mice were fasted for 8 hours before euthanasia. Total cholesterol and triglyceride levels in plasma samples were quantified using a cholesterol/cholesteryl ester assay kit (ab65359, Abcam) and a triglyceride assay kit (ab65336, Abcam), respectively, according to manufacturer's protocol.

Aorta single-cell suspension

Aortae were perfused with 10 mL cold PBS containing 2 mM EDTA. After removal of the surrounding fat and connective tissue, aortae were cut into several segments and digested in the aorta digestion enzyme solution [1] [HBSS containing 250U /mL collagenase type XI (C7657, Sigma Aldrich), 120 U/mL hyaluronidase type I-s (H3506, Sigma Aldrich), 120 U/mL DNase I (DN25, Sigma Aldrich), and 450 U/mL collagenase type I (SCR103, Sigma Aldrich)] for 60 minutes at 37°C. The digested aortae were then passed through a 70 μM cell strainer (25-376, Olympus Plastics), and cells were pelleted by centrifugation and resuspended in RPMI containing 0.5% Poloxamer 188 (24040032, Thermo Fisher Scientific).

Flow cytometry-based detection of inflammarafts

Aortic single-cell suspensions were incubated at 37°C for 30 minutes for cell surface recovery following enzymatic digestion and stained with Ghost Dye Red 780 Fixable Viability Dye (18452, Cell Signaling Technology). After neutral lipid staining with 1 μg/mL BODIPY 505/515 (D3921, Thermo Fisher Scientific), the single-cell suspensions were fixed with 4% PFA at 4°C for 20

minutes. Cells were blocked with an anti-CD16/CD32 antibody (553142, BD Biosciences) in PBS containing 2% BSA on ice for 30 minutes and then incubated with a mixture of BV650-conjugated anti-CD45 antibody (103151, Biolegend), PerCP/Cy5.5-conjugated anti-F4/80 antibody (123128, Biolegend), AF594-Conjugated anti-Cholera Toxin Subunit B antibody (C22842, Invitrogen), APC-conjugated anti-TLR4 (145406, BioLegend; detecting total TLR4 expression) antibody, and PE-conjugated anti-TLR4/MD-2 (Invitrogen, 12-9924-81; detecting TLR4 monomers) antibody for 60 minutes on ice. Cells were analyzed on a CytoFLEX Flow Cytometer (Beckman Coulter). The percentage of TLR4 dimers was calculated from geometric mean fluorescence intensities of PE-conjugated TLR4/MD2 antibody (monomers) and APC-conjugated TLR4 antibody (total). Splenic F4/80-positive macrophages obtained from *Ldlr*$^{-/-}$ mice fed a standard laboratory diet were treated for 15 minutes with 100 ng/ml LPS (to induce transient TLR4 dimerization) and served as a positive control for the TLR4 dimerization assay. Non-stimulated splenic macrophages served as a negative control to standardize data obtained over time.

Statistical Analyses

Data are presented as mean ± SEM. N represents biological replicates. Data were analyzed for normality and equal variance using the Kolmogorov-Smirnov test. A two-sided Student's *t*-test was employed to compare two groups. For multiple-group comparisons with one or two independent factors, one-way or two-way ANOVA was conducted with Tukey's or Dunnett's multiple comparison tests for normally distributed variables. All statistical analyses were performed using GraphPad Prism version 9.4.1. A p-value of less than 0.05 was considered statistically significant.

Results

Increased inflammarafts in lesional macrophage foam cells in AIBP-deficient mice

Aortic single-cell suspensions from *Apoa1bp*$^{-/-}$*Ldlr*$^{-/-}$ and *Ldlr*$^{-/-}$ mice fed a 16-week high-fat diet were gated for BODIPY-high (foamy) and BODIPY-low (non-foamy), CD45^{+}F4/80^{+} macrophages (Supplemental Figure S1). The number of macrophage foam cells was significantly increased in *Apoa1bp*$^{-/-}$*Ldlr*$^{-/-}$ mice when compared to *Ldlr*$^{-/-}$ mice (Figure 1A and 1F). Moreover, *Apoa1bp*-deficient macrophage foam cells had more neutral lipid accumulated, measured by BODIPY intensity, than *Ldlr*$^{-/-}$ foam cells (Figure 1B and 1G). Quantitative analysis revealed an elevated expression of TLR4 dimers in both macrophage foam cells and non-foamy macrophages from *Apoa1bp*$^{-/-}$*Ldlr*$^{-/-}$ mice when compared to those from *Ldlr*$^{-/-}$ mice (Figure 1C and 1H). Integration of TLR4 dimers (TLR4 dimers multiplied by the percentage of macrophage subtypes) showed that macrophage foam cells in *Apoa1bp*$^{-/-}$*Ldlr*$^{-/-}$ male mice are the major cell type expressing inflammarafts. In contrast, in *Ldlr*$^{-/-}$ mice, non-foamy macrophages were the major TLR4 dimer-expressing cell type (Figure 1D and 1I). Furthermore, *Apoa1bp*$^{-/-}$*Ldlr*$^{-/-}$ macrophage foam cells exhibited increased levels of lipid rafts, equal to lipid raft levels in non-foamy macrophages in both *Apoa1bp*$^{-/-}$*Ldlr*$^{-/-}$ and *Ldlr*$^{-/-}$ mice (Figure 1E and 1J). These results indicate that AIBP deficiency leads to increased TLR4 dimer-containing lipid raft expression in macrophage foam cells, making them the major inflammaraft-expressing subpopulation in atherosclerotic plaques in AIBP-deficient mice.

Advanced atherosclerosis in AIBP-deficient mice

To assess the extent of atherosclerosis, consecutive cross-sections were collected from the aortic root for quantification. Larger atherosclerotic lesions were observed in the proximal region of the aortic valve in *Apoa1bp*$^{-/-}$*Ldlr*$^{-/-}$ male mice when compared to control mice (Figure 2A, 2B). AIBP-

deficient female mice displayed a larger distal (500 to 600 μm from valve origin) lesion size (Figure 2A, 2C). The analysis of total lesion volume indicated a tendency for increased atherosclerotic plaque burden (Figure 2D). We observed sex differences in the atherosclerotic lesion morphology in *Apoa1bp*$^{-/-}$*Ldlr*$^{-/-}$ mice (Figure 2B, 2C). In *Ldlr*$^{-/-}$ mice, the lesion size curves in both males and females were bell-shaped, peaking at 400 μm from the aortic root. In *Apoa1bp*$^{-/-}$*Ldlr*$^{-/-}$ mice, the lesion size curve in female mice continuously ascended all the way from the valve origin to the 600 μm distance, while the curve in male mice remained bell-shaped, peaking at 500 μm.

Formation and enlargement of a central necrotic core indicate advanced atherosclerotic plaques and imply plaque destabilization, associated with vascular inflammation. [14,15] Consistent with the lesion size measurements, a larger necrotic core size was observed in the proximal region of the aortic valve in *Apoa1bp*$^{-/-}$*Ldlr*$^{-/-}$ male mice (Figure 2A, 2E) and at the distal region of the aortic valve in *Apoa1bp*$^{-/-}$*Ldlr*$^{-/-}$ female mice (Figure 2A, 2F) when compared to *Ldlr*$^{-/-}$ mice. Of note, the total necrotic core volume was significantly higher in *Apoa1bp*$^{-/-}$*Ldlr*$^{-/-}$ mice than in *Ldlr*$^{-/-}$ mice, in both male and female, suggesting a more vulnerable advanced plaque in AIBP-deficient mice (Figure 2G).

Apoa1bp$^{-/-}$*Ldlr*$^{-/-}$ mice gained body weight faster than *Ldlr*$^{-/-}$ mice and had higher plasma triglyceride but not cholesterol levels (Supplemental Figure S2A-S2D). Overall, male and female mice showed similar results (Figure 1F-J, Supplemental Figure S2A-S2D). These results indicate that AIBP deficiency affects lipid homeostasis and leads to a larger lesion burden and advanced atherosclerotic plaques.

Discussion

In this study, we demonstrated that the atheroprotective effect of AIBP is strongly associated with the attenuation of TLR4 inflammarafts in macrophage foam cells. Unexpectedly, AIBP deficiency leads to both marked expression of inflammarafts and increased lipid accumulation in lesional macrophage foam cells. Advanced atherosclerotic plaques accompanied the transition of foam cells to a proinflammatory phenotype.

These findings were surprising because multiple lines of evidence support the concept that macrophage foam cells express lipid storage genes is associated with suppressed expression of inflammatory-response genes, leading to the reduced contribution of foam cells to inflammation in atherosclerosis compared to non-foamy macrophages. Macrophage foam cells from *Ldlr*$^{-/-}$ mice exhibit altered cholesterol metabolism and a marked suppression of proinflammatory mediators that are normally characteristic of the inflammatory responses associated with atherosclerotic lesions. [16] Similarly, transcriptome data from *Apoe*$^{-/-}$ mice show that lipid-rich macrophage foam cells express few inflammatory genes but many lipid-processing genes, while non-foamy macrophages are the primary population expressing IL-1β and other inflammatory mediators in the atherosclerotic aorta. [1] Moreover, we previously established that non-foamy macrophages in atherosclerotic lesions of *Ldlr*$^{-/-}$ mice express higher levels of inflammarafts than macrophage foam cells, correlating with increased plasma levels of the inflammatory cytokines MCP-1 (monocyte chemoattractant protein-1), interleukin (IL)-6, and IL-1β. [3]

Despite the evidence for a non-inflammatory character of macrophage foam cells, the mechanisms by which macrophage foam cells in atherosclerotic lesions exhibit less inflammatory response than other macrophage populations remain poorly understood. The most notable difference between foam cells and non-foamy macrophages is the content of intracellular lipid

droplets, as well as distinct lipid metabolism. High levels of desmosterol, the last intermediate in the Bloch pathway of cholesterol biosynthesis, have been reported to be associated with suppression of proinflammatory mediators in macrophage foam cells via several homeostatic pathways, including activation of LXR target genes, inhibition of SREBP target genes, and selective reprogramming of fatty acid metabolism. [16] These findings indicate that lipid metabolism is involved in the suppression of inflammatory mediators.

AIBP not only facilitates cholesterol efflux from the cell membrane to regulate lipid metabolism, but AIBP-mediated disruption of lipid rafts also protects microglia from TLR4 inflammaraft-associated oxidative stress and mitochondrial dysfunction. [12] In our study, we observed that AIBP deficiency leads to enhanced expression of TLR4 dimers and lipid rafts in macrophage foam cells, as well as increased lipid accumulation in lesional macrophages, resulting in macrophage foam cells being the major inflammatory macrophage subpopulation in atherosclerotic lesions of *Apoa1bp*$^{-/-}$*Ldlr*$^{-/-}$ mice. In addition, the transition of foam cells to a proinflammatory phenotype is accompanied by advanced atherosclerotic plaques. Based on these findings, we propose that macrophage foam cells can become inflammatory and that AIBP suppresses this proinflammatory phenotype by disrupting TLR4 inflammarafts and reducing oxidative stress induced by excessive cholesterol accumulation.

Interestingly, our analysis of aortic root lesions showed a sex difference in lesion distribution in response to AIBP deficiency. Female *Apoa1bp*$^{-/-}$*Ldlr*$^{-/-}$ mice exhibited a continuous increase in lesion size and necrotic core size starting from the origin of the aortic valve, while lesions in male *Apoa1bp*$^{-/-}$*Ldlr*$^{-/-}$ mice and both sexes of *Ldlr*$^{-/-}$ mice reached the maximum size at 400-500 μm from the origin. These findings indicate that AIBP contributes to the sex difference observed in atherosclerosis. [17,18]

The choice of a systemic *Apoa1bp*$^{-/-}$*Ldlr*$^{-/-}$ mouse for this study was dictated by the secreted nature of ubiquitously expressed AIBP, which exerts its major effect on lipid rafts extracellularly. We have conducted an atherosclerosis study with macrophage-specific *Apoa1bp-LysM-cre Ldlr*$^{-/-}$ vs. *Ldlr*$^{-/-}$ mice and received results similar to those with systemic *Apoa1bp*$^{-/-}$*Ldlr*$^{-/-}$ mice (unpublished). In our previous study with *Apoa1bp*$^{-/-}$*Ldlr*$^{-/-}$ mice, we observed elevated plasma cholesterol and triglyceride levels,[11] in contrast to the results of this work, which showed increased triglyceride but not cholesterol plasma levels. The likely reason for this difference is the difference in the high-fat diets used in these two studies. The Western diet used in the previous study contained 1.25% cholesterol [11], which is higher than the 0.2% cholesterol diet in this study.

The major finding of this study – that AIBP suppresses TLR4 inflammaraft expression specifically in macrophage foam cells – warrants a detailed, genome-wide analysis of gene expression in foamy and non-foamy macrophages from *Apoa1bp*$^{-/-}$*Ldlr*$^{-/-}$ and *Ldlr*$^{-/-}$ mice. This will help elucidate the mechanisms by which AIBP regulates TLR4 inflammarafts and the signaling pathways in macrophage foam cells that prevent them from assuming an inflammatory phenotype.

Acknowledgments

The authors thank Dr Nicholas Webster for generously sharing access to a flow cytometer in his lab.

Sources of Funding

This study was supported by National Institutes of Health (NIH) grants HL171505 and HL136275 (to Y.I.M.) and DK126848, HD106463, and GM128777 (to P.L.S.M.G).

Disclosures

Y.I.M. is a scientific co-founder of Raft Pharmaceuticals LLC. The terms of this arrangement have been reviewed and approved by the University of California, San Diego, in accordance with its conflict-of-interest policies. Other authors declare no competing interests.

Supplemental Material

Supplemental Figures S1 and S2

Major Resources Table

References

1. Kim K, Shim D, Lee JS, Zaitsev K, Williams JW, Kim K-W, Jang M-Y, Jang HS, Yun TJ, Lee SH, et al. Transcriptome Analysis Reveals Nonfoamy Rather Than Foamy Plaque Macrophages Are Proinflammatory in Atherosclerotic Murine Models. *Circulation Research*. 2018;123:1127-1142. doi: doi:10.1161/CIRCRESAHA.118.312804
2. Li C, Qu L, Matz AJ, Murphy PA, Liu Y, Manichaikul AW, Aguiar D, Rich SS, Herrington DM, Vu D, et al. AtheroSpectrum Reveals Novel Macrophage Foam Cell Gene Signatures Associated With Atherosclerotic Cardiovascular Disease Risk. *Circulation*. 2022;145:206-218. doi: doi:10.1161/CIRCULATIONAHA.121.054285
3. Navia-Pelaez JM, Agatisa-Boyle C, Choi S-H, Kim YS, Li S, Alekseeva E, Weldy K, Miller YI. Differential Expression of Inflammarafts in Macrophage Foam Cells and in Nonfoamy Macrophages in Atherosclerotic Lesions—Brief Report. *Arteriosclerosis, Thrombosis, and Vascular Biology*. 2023;43:323-329. doi: 10.1161/ATVBAHA.122.318006
4. Miller YI, Navia-Pelaez JM, Corr M, Yaksh TL. Lipid rafts in glial cells: role in neuroinflammation and pain processing. *J Lipid Res*. 2020;61:655-666. doi: 10.1194/jlr.TR119000468
5. Anttila V, Winsvold BS, Gormley P, Kurth T, Bettella F, McMahon G, Kallela M, Malik R, de Vries B, Terwindt G, et al. Genome-wide meta-analysis identifies new susceptibility loci for migraine. *Nature Genetics*. 2013;45:912-917. doi: 10.1038/ng.2676
6. Zhang M, Li L, Xie W, Wu J-F, Yao F, Tan Y-L, Xia X-D, Liu X-Y, Liu D, Lan G, et al. Apolipoprotein A-1 binding protein promotes macrophage cholesterol efflux by facilitating apolipoprotein A-1 binding to ABCA1 and preventing ABCA1 degradation. *Atherosclerosis*. 2016;248:149-159. doi: 10.1016/j.atherosclerosis.2016.03.008
7. Matsuo M. ABCA1 and ABCG1 as potential therapeutic targets for the prevention of atherosclerosis. *J Pharmacol Sci*. 2022;148:197-203. doi: 10.1016/j.jphs.2021.11.005
8. Ritter M, Buechler C, Boettcher A, Barlage S, Schmitz-Madry A, Orso E, Bared SM, Schmiedeknecht G, Baehr CH, Fricker G, et al. Cloning and characterization of a novel apolipoprotein A-I binding protein, AI-BP, secreted by cells of the kidney proximal tubules in response to HDL or ApoA-I. *Genomics*. 2002;79:693-702. doi: 10.1006/geno.2002.6761
9. Choi S-H, Agatisa-Boyle C, Gonen A, Kim A, Kim J, Alekseeva E, Tsimikas S, Miller YI. Intracellular AIBP (Apolipoprotein A-I Binding Protein) Regulates Oxidized LDL (Low-Density Lipoprotein)-Induced Mitophagy in Macrophages. *Arteriosclerosis, Thrombosis, and Vascular Biology*. 2021;41:e82-e96. doi: doi:10.1161/ATVBAHA.120.315485
10. Duan M, Chen H, Yin L, Zhu X, Novák P, Lv Y, Zhao G, Yin K. Mitochondrial apolipoprotein A-I binding protein alleviates atherosclerosis by regulating mitophagy and macrophage polarization. *Cell Communication and Signaling*. 2022;20:60. doi: 10.1186/s12964-022-00858-8
11. Schneider DA, Choi SH, Agatisa-Boyle C, Zhu L, Kim J, Pattison J, Sears DD, Gordts P, Fang L, Miller YI. AIBP protects against metabolic abnormalities and atherosclerosis. *J Lipid Res*. 2018;59:854-863. doi: 10.1194/jlr.M083618
12. Kim YS, Choi S-H, Kim K-Y, Navia-Pelaez JM, Perkins GA, Choi S, Kim J, Nazarenkov N, Rissman RA, Ju W-K, et al. AIBP controls TLR4 inflammarafts and mitochondrial

dysfunction in a mouse model of Alzheimer's disease. *Journal of Neuroinflammation*. 2024;21:245. doi: 10.1186/s12974-024-03214-4
13. Woller SA, Choi S-H, An EJ, Low H, Schneider DA, Ramachandran R, Kim J, Bae YS, Sviridov D, Corr M, et al. Inhibition of Neuroinflammation by AIBP: Spinal Effects upon Facilitated Pain States. *Cell Reports*. 2018;23:2667-2677. doi: 10.1016/j.celrep.2018.04.110
14. De Meyer GRY, Zurek M, Puylaert P, Martinet W. Programmed death of macrophages in atherosclerosis: mechanisms and therapeutic targets. *Nature Reviews Cardiology*. 2024;21:312-325. doi: 10.1038/s41569-023-00957-0
15. Puylaert P, Zurek M, Rayner KJ, De Meyer GRY, Martinet W. Regulated Necrosis in Atherosclerosis. *Arteriosclerosis, Thrombosis, and Vascular Biology*. 2022;42:1283-1306. doi: doi:10.1161/ATVBAHA.122.318177
16. Spann NJ, Garmire LX, McDonald JG, Myers DS, Milne SB, Shibata N, Reichart D, Fox JN, Shaked I, Heudobler D, et al. Regulated accumulation of desmosterol integrates macrophage lipid metabolism and inflammatory responses. *Cell*. 2012;151:138-152. doi: 10.1016/j.cell.2012.06.054
17. Yerly A, van der Vorst EPC, Baumgartner I, Bernhard Sarah M, Schindewolf M, Döring Y. Sex-specific and hormone-related differences in vascular remodelling in atherosclerosis. *European Journal of Clinical Investigation*. 2023;53:e13885.
18. Man JJ, Beckman JA, Jaffe IZ. Sex as a Biological Variable in Atherosclerosis. *Circulation Research*. 2020;126:1297-1319. doi: doi:10.1161/CIRCRESAHA.120.315930

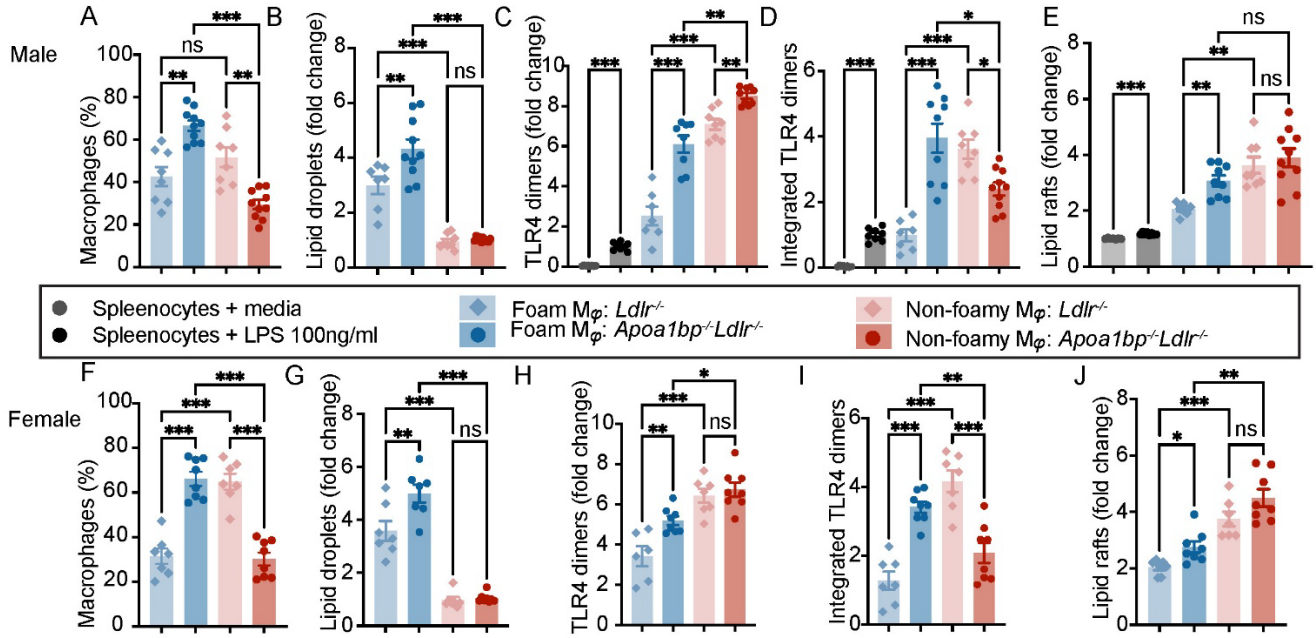

Figure 1. Foam cells are the major population expressing TLR4 inflammarafts in AIBP-deficient mice. A-E. Data from male mice (n=8-10). **F-J.** Data from female mice (n=7-8). **A/F.** Percentages of foam cells and non-foamy macrophages in atherosclerotic lesions from *Apoa1bp*$^{-/-}$ *Ldlr*$^{-/-}$ and *Ldlr*$^{-/-}$ mice. **B/G.** Content of neutral lipids in foam cells, normalized to the readings in non-foamy macrophages from the same aorta **C/H.** Expression of TLR4 dimers in foam cells and non-foamy macrophages in *Apoa1bp*$^{-/-}$*Ldlr*$^{-/-}$ and *Ldlr*$^{-/-}$ mice. Splenocytes stimulated with vehicle or LPS (100 ng/ml, 15 min) served as negative and positive controls in **C-D** and **H-I**. **D/I**. Integrated TLR4 dimers (TLR4 dimers in each cell type in **C/H** multiplied by cell type percentage in **A/F**. **E/J**. Expression of lipid rafts in lesional macrophages. One-way ANOVA with Tukey's. Mean ± SEM; ns, nonsignificant; *, $p \leq 0.05$; **, $p \leq 0.01$; ***, $p \leq 0.001$.

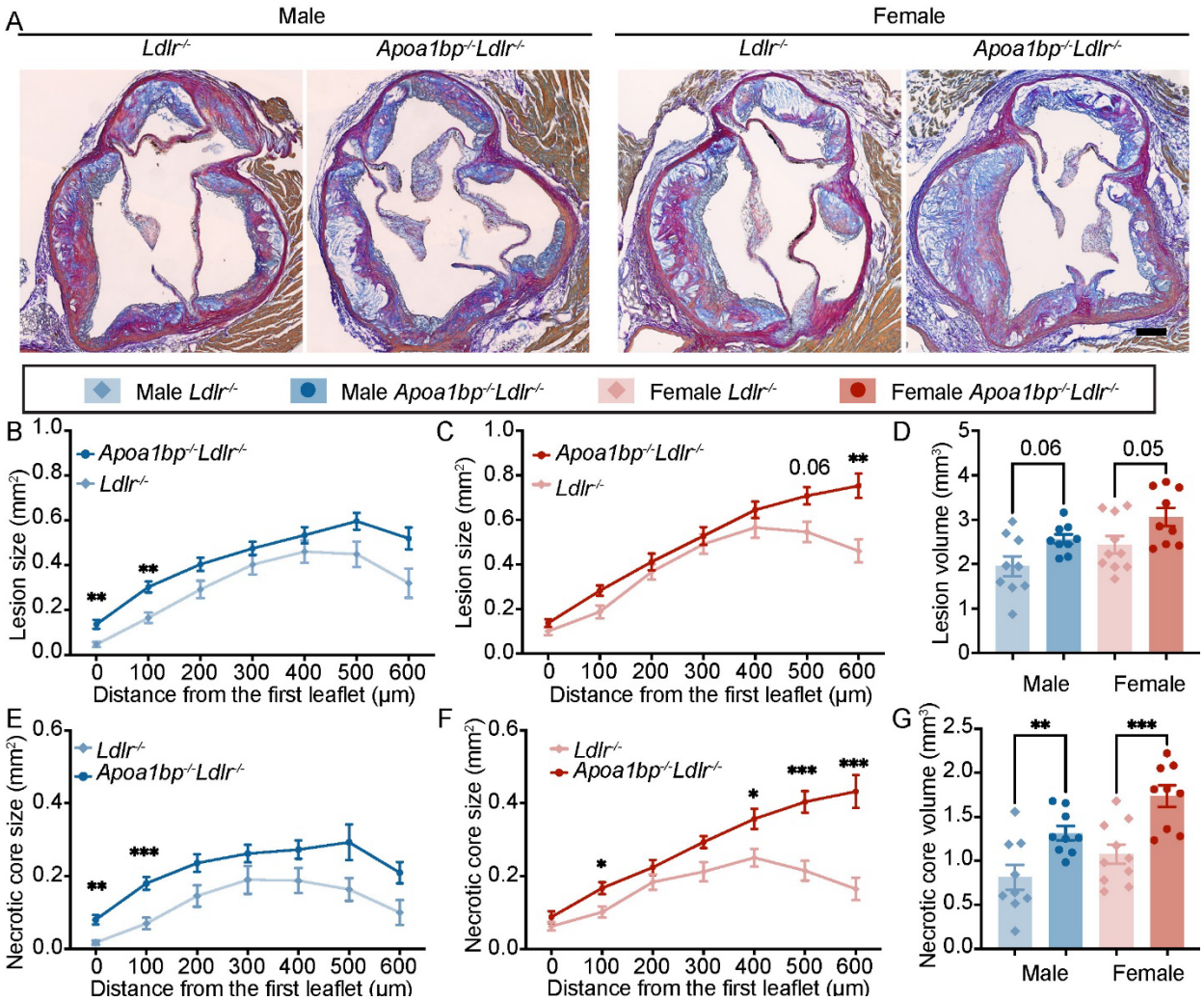

Figure 2. Advanced atherosclerotic lesions in AIBP-deficient mice. A. Representative images of the aortic root stained with modified Van Gieson staining. Scale bar = 10 μm. Quantitative analysis of lesion size in male mice (**B**) and female mice (**C**). **D**. Lesion volume measured by area under the curve from **B** and **C**. Quantitative analysis of necrotic core size in male mice (**E**) and female mice (**F**). **G.** Necrotic core volume measured by area under the curve from **E** and **F**. N = 9-10; two-way ANOVA with Tukey's or Dunnett's multiple comparison tests (B, C, E, F), and t-test (D and G). Mean ± SEM; ns, nonsignificant; *, $p \leq 0.05$; **, $p \leq 0.01$; ***, $p \leq 0.001$.

Supplemental Material

Increased atherosclerosis and expression of inflammarafts in macrophage foam cells in AIBP-deficient mice

Shenglin Li, Nicolaus Nazarenkov, Elena Alekseeva, Juliana M. Navia-Pelaez, Patrick Secrest, Philip L.S.M. Gordts, Sven Heinz, Yury I. Miller

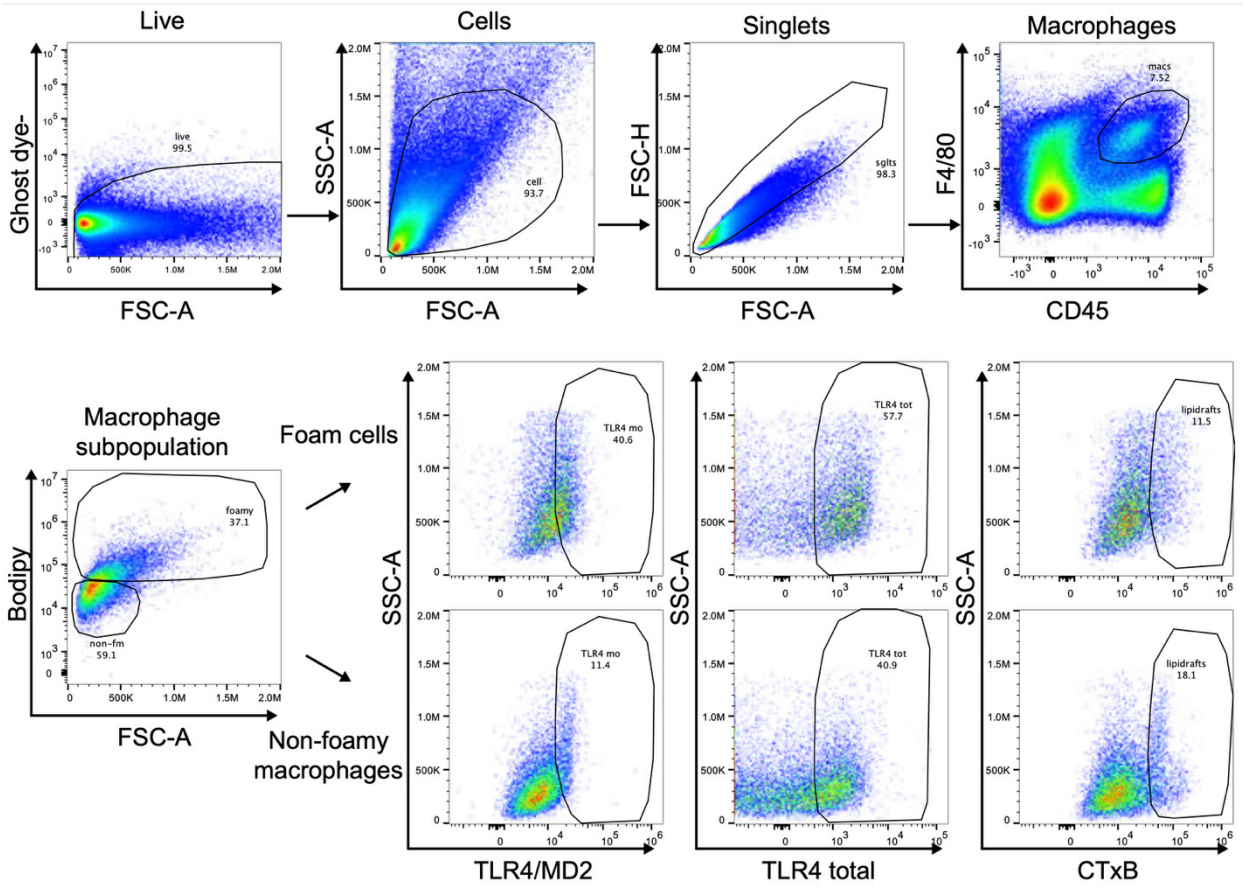

Supplemental Figure 1. Gating strategy for expression of TLR4 dimers and lipid rafts. Aortic single-cell suspensions from *Apoa1bp*$^{-/-}$*Ldlr*$^{-/-}$ and *Ldlr*$^{-/-}$ mice fed a 16-week high-fat diet were gated for BODIPY-high foamy and BODIPY-low non-foamy, CD45^{+} F4/80^{+} macrophages. The percentage of TLR4 dimers was calculated from geometric mean fluorescence intensities of PE-conjugated TLR4/MD2 antibody (monomers) and APC-conjugated TLR4 antibody (total). Lipid rafts were calculated from the geometric mean fluorescence intensity of AF594-conjugated cholera toxin B subunit.

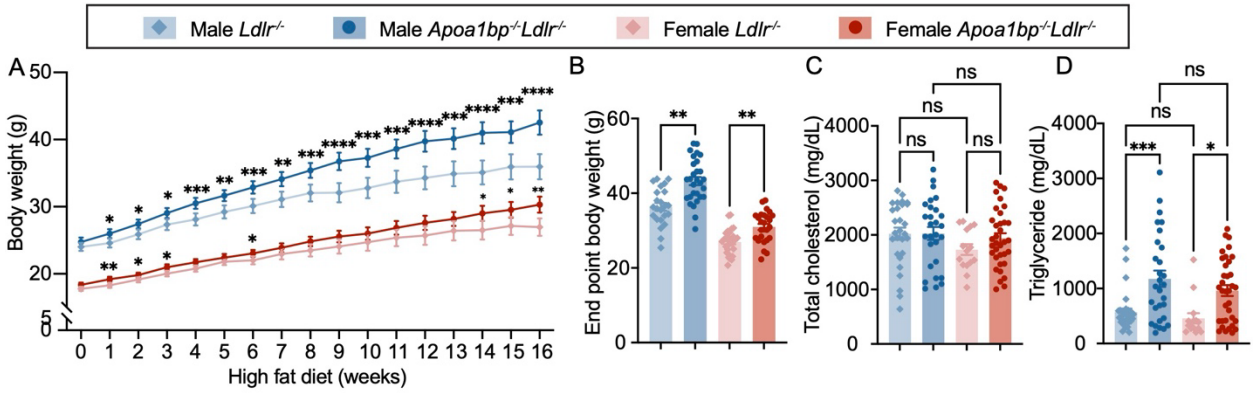

Supplemental Figure 2. Weight gain and plasma lipid levels. A. Body weight changes of *Apoa1bp*$^{-/-}$*Ldlr*$^{-/-}$ and *Ldlr*$^{-/-}$ mice, starting from week 0 to week 16th. **B.** End point body weight. **C.** Plasma total cholesterol levels. **D.** Plasma triglyceride levels. N = 9-10; two-way and one-way ANOVA with Tukey's or Dunnett's multiple comparison tests for statistical analysis. Results are presented as Mean ± SEM; ns, nonsignificant; *, $p \leq 0.05$; **, $p \leq 0.01$; ***, $p \leq 0.001$.

Major Resources Table

Animals (in vivo studies)

Species	Vendor or Source	Background Strain	Sex	Persistent ID / URL
Ldlr$^{-/-}$	The Jackson Lab	C57/BL6	Male & female	002207

Genetically Modified Animals

	Species	Vendor or Source	Background Strain	Other Information	Persistent ID / URL
Parent - Male	*Apoa1bp*$^{-/-}$ *Ldlr*$^{-/-}$	In house	C57/BL6		n/a
Parent - Female	*Apoa1bp*$^{-/-}$ *Ldlr*$^{-/-}$	In house	C57/BL6		n/a

Antibodies

Target antigen	Vendor or Source	Catalog #	Working concentration	Persistent ID / URL
Purified Rat Anti-Mouse CD16/CD32	BD Biosciences	553142	20 µg/mL	https://www.bdbiosciences.com/en-us/products/reagents/western-blotting-and-molecular-reagents/purified-rat-anti-mouse-cd16-cd32-mouse-bd-fc-block.553141?tab=product_details

Brilliant Violet 650™ anti-mouse CD45	Biolegend	103151	4 µg/mL	https://www.biolegend.com/en-us/products/brilliant-violet-650-anti-mouse-cd45-antibody-11987
PerCP/Cyanine5.5 anti-mouse F4/80 Antibody	Biolegend	123128	4 µg/mL	https://www.biolegend.com/en-us/products/percp-cyanine5-5-anti-mouse-f480-antibody-4303
TLR4/MD-2 Complex Monoclonal Antibody (MTS510), PE	Invitrogen	12-9924-81	4 µg/mL	https://www.thermofisher.com/antibody/product/TLR4-MD-2-Complex-Antibody-clone-MTS510-Monoclonal/12-9924-81
APC anti-mouse CD284 (TLR4) Antibody	Biolegend	145406	4 µg/mL	https://www.biolegend.com/en-us/products/apc-anti-mouse-cd284-tlr4-antibody-8871
Cholera Toxin Subunit B, Alexa Fluor™ 594 Conjugate	Invitrogen	C22842	4 µg/mL	https://www.thermofisher.com/order/catalog/product/C22842?SID=srch-hj-C22842
BODIPY 505/515	Thermo Fisher	D3921	1 µg/mL	https://www.thermofisher.com/order/catalog/product/D3921?SID=srch-hj-D3921

Other

Description	Vendor or Source	Catalog #	Working concentration	Persistent ID / URL
collagenase type XI	Sigma Aldrich	C7657	250U/mL	https://www.sigmaaldrich.com/US/en/product/sigma/c7657
hyaluronidase type I-s	Sigma Aldrich	H3506	120U/mL	https://www.sigmaaldrich.com/US/en/product/sigma/h3506
DNase I	Sigma Aldrich	DN25	120U/mL	https://www.sigmaaldrich.com/US/en/product/sigma/dn25
collagenase type I	Sigma Aldrich	SCR103	450U/mL	https://www.sigmaaldrich.com/US/en/product/mm/scr103